Lawrence Berkeley National Laboratory
LBL Publications

Title
Preparing for the Next Generation of EUV Lithography at the Center for X-ray Optics

Permalink
https://escholarship.org/uc/item/07h5f8vn

Journal
Synchrotron Radiation News, 32(4)

ISSN
0894-0886

Authors
Miyakawa, Ryan
Naulleau, Patrick

Publication Date
2019-07-04

DOI
10.1080/08940886.2019.1634432

Peer reviewed

eScholarship.org Powered by the California Digital Library
University of California

Preparing for the Next Generation of EUV Lithography at the Center for X-ray Optics

Ryan Miyakawa and PatRick Naulleau
Center for X-ray Optics, Berkeley, California, USA

The introduction of EUV lithography into high-volume semiconductor manufacturing this year represents a monumental milestone for EUV technology. After nearly 30 years of development, the EUV research community has overcome many of the key obstacles required to enable the long-awaited integration of EUV lithography into the lab. These obstacles have included: the development of a stable, high-powered EUV source to ensure adequate exposure tool reliability; controlling EUV mask defects and mask contamination; and the development of EUV resists with adequate sensitivity, resolution, and line width roughness to meet the tolerances required for high-volume manufacturing.

As EUV moves into its second generation, there will be new challenges facing the community as it works to push EUV technology into the future [1]. Smaller feature sizes will be achieved using higher numerical aperture optics, which are planned to have an anamorphic geometry (asymmetric magnification and numerical aperture between horizontal and vertical axes) to overcome 3D effects at the mask [2]. This new geometry and its larger angle ranges make understanding mask absorber and multilayer effects all the more important. New methods for high-NA wavefront metrology need to be tested to ensure that these optical systems can be aligned to operate with minimal aberrations. Mask defects need to continue to be studied, and the inclusion of EUV pellicles [3] in the roadmap requires that mask inspection and review systems adapt accordingly. Finally, new resists must be developed to support the increased resolution of feature sizes below 8 nm half pitch.

The Center for X-ray Optics (CXRO) at Berkeley Lab has been a leader in EUV research for the past 25 years. Leveraging 13.5 nm EUV light from the Advanced Light Source synchrotron facility, CXRO is home to several EUV and soft X-ray (SXR) research tools that have provided important insights into EUV resists, masks, and coatings. The 0.3 NA Microfield exposure tool (MET) and Dose Calibration Tool (DCT) have played an instrumental role in the development of the current generation of high-resolution EUV resists. The Actinic Inspection Tool (AIT) and its successor, SHARP, have enabled aerial image analysis, providing key insights into mask defects, 3D mask effects, illumination, and aberrations. And the CXRO Reflectometer continues to be the industry standard in multilayer coating and EUV mask scattering metrology.

To address the new challenges facing the next generation of EUV lithography, CXRO has upgraded its suite of EUV research tools. The 0.5 NA MET5 is a newly commissioned projection lithography tool that is capable of printing feature sizes down to 8 nm half pitch. A new radiation chemistry program is deploying several techniques aimed at dissecting the role of primary photoelectrons and secondary electrons in EUV resists. The SHARP microscope has been outfitted with anamorphic zone plate lenses that can emulate the geometry of next-generation EUV scanners, and the reflectometer has been applied to new scattering experiments for the purpose of understanding the 3D effects of EUV mask multilayers, as well as determining mask properties using scattering profiles. In parallel with these tools, the CXRO High-NA Wavefront Sensing Program is developing high-resolution wavefront sensors suitable for measuring aberrations at high NA. This article presents an overview of these programs and describes how they will address the primary challenges that face the EUV community as it moves to the next generation of EUV lithography.

MET5 and DCT: Supporting high-resolution EUV resist development

Next-generation EUV lithography requires ultra-high-resolution photoresists with sufficient sensitivity and line-width roughness (LWR) [4]. Research tools like the Berkeley MET3, Berkeley MET5, and Dose Calibration Tool (DCT) play a pivotal role in providing a means for resist manufacturers to characterize resist properties.

The Berkeley MET5

The Berkeley MET and DCT platforms have been supporting leading-edge EUV resist development since 2004, with over 14,000 material processes tested. In 2018, the new Berkeley MET5 was commissioned at Beamline 12.0.1.4 of the Advanced Light Source synchrotron facility at Berkeley Lab alongside its predecessor, the MET3. With its 0.5 NA Schwarzschild objective, the MET5 is capable of creating sufficient aerial image contrast to resolve dense line/space patterns down to 8 nm half pitch [5]. Figure 1a shows SEM images of exposed Inpria resist at a dose of 40 mJ/cm^2, demonstrating print resolution at

the ultimate resolution of the tool.

The MET5 has an aberration-corrected field size of 200 µm by 30 µm. Focus control is assisted by a 6-channel laser-based height sensor with 0.1 nm resolution. The optical subframe is mounted on a floating vibration isolated platform. Additional active vibration isolation and lateral drift control are enabled via a displacement measuring interferometer (DMI) system that tracks the reticle and wafer motion with respect to the optical housing at 1 KHz with 0.1 nm resolution. These controls allow the system drift and vibration to be stable to better than 1 nm rms in X, Y, and Z.

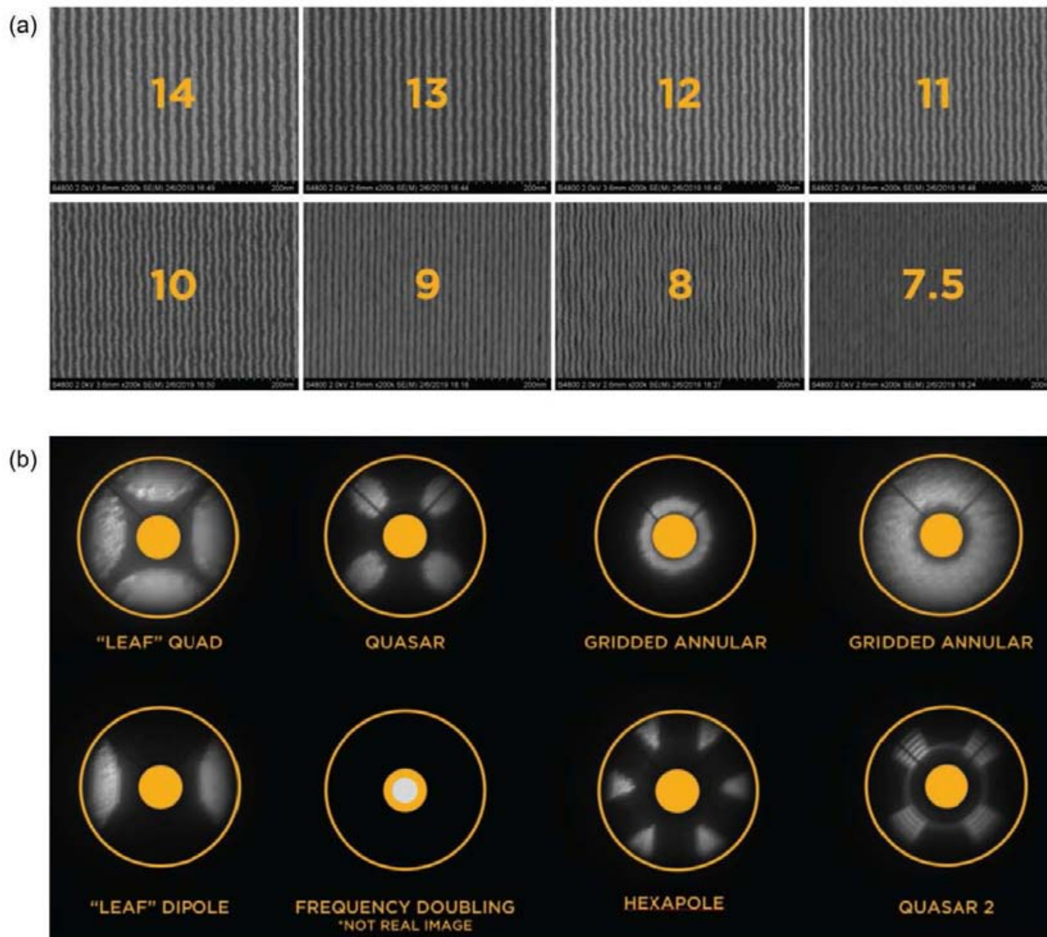

Figure 1: (a) SEM images of Inpria resist exposed by MET5 showing print resolution down to 8 nm half pitch; (b) examples of pupil fill illuminations on MET5 from its lossless Fourier synthesis illumination module.

Illumination partial coherence (pupil fill) settings are important for resist development, as they affect aerial image contrast for various feature types. Next-generation EUV scanners, such as from ASML [6], leverage source-mask optimized illumination, which requires the ability to create free-form pupil fills. The MET5 accommodates this need by featuring a fully programmable, lossless Fourier synthesis illuminator capable of generating arbitrary pupil fill illuminations, including annular, dipole, quadrupole, quasar, and free-form illuminations. Figure 1b shows pupil grams of various illuminations demonstrating this capability.

To ensure that the high-NA optic is performing near its diffraction limit, an in-situ wavefront sensor module featuring a lateral shearing interferometer is installed alongside the wafer module. A long-range translation stage allows these modules to toggle back and forth without breaking the system vacuum. When the optic was initially installed, the wavefront was measured to have an aberration level of 0.87 nm rms ($Z_4 - Z_{37}$) at the center of the field. The optic was subsequently aligned and its aberrations were reduced to 0.31 nm rms, below the acceptance specification of 0.5 nm rms. Details of the lateral shearing interferometer are discussed in a later section.

Dose Calibration Tool (DCT)

The Dose Calibration Tool (DCT) is a dose-calibrated clear field exposure tool designed to characterize resist contrast curves and sensitivity. Instead of imaging a clear field to the wafer, the DCT illuminates an aperture that casts a shadow onto the wafer. Like the MET5, the DCT is powered by the same synchrotron beam at 13.5 nm wavelength, but since the optical geometry is much simpler, the DCT can support a throughput of six wafers per hour, compared to two wafers per hour for MET5. A calibrated photodiode can be inserted into the beam so that contrast curves can be reported in absolute dose numbers. A scanning mirror upstream of the DCT aperture ensures uniformity across the clear field, which can be as large as 1 cm^2.

The DCT acts as a complementary tool to MET5; users interested in measuring the sensitivity of a series of resists might use the DCT, whereas users also interested in the resolution and LWR properties of the resist would use MET5. To date, the DCT has characterized over 5000 resist and underlayer combinations.

Radiation chemistry characterization

CXRO and the ALS host a suite of EUV resist radiation chemistry tools critical to gaining fundamental understanding of the EUV exposure process. This understanding can help guide the development of EUV resists and underlayers that can support the resolution, sensitivity, and LWR required by next-generation EUV lithography. Two techniques that are useful for studying radiation chemistry are photoelectron spectroscopy and resonant soft X-ray scattering (RSoXS).

Photoelectron spectroscopy of EUV resist materials

The exposure of an EUV resist happens in two stages. The first is the absorption of EUV photons and the generation of primary electrons via photoemission, and the second is the subsequent interaction between these primary electrons and the resist causing the generation of secondary electrons, which are believed to be responsible for the bulk of the resist chemistry.

To study the first step, a gas phase spectrometer [7] has been developed that allows resist materials or constituent components to be formed into a molecular or nanoparticle beam and irradiated with EUV light. The system uses an electron spectrometer to directly measure the generated primary electron spectrum and a mass spectrometer to measure the fragmentation spectrum. By quantifying the performance of several molecules in terms of photoemission cross-sections and electron yield per primary photoionization event, this work can potentially identify candidates for new resist formulations.

Since the gas phase spectrometer works on isolated specimens, it cannot be used to study the secondary electrons in resist. For this reason, a condensed phase electron spectrometer system [8] is being used to study this second step of the exposure process. In this system, a resist-coated silicon wafer is irradiated with EUV light and the emitted electron spectrum is measured. Computational methods are used to relate this emitted spectrum to the internal secondary electron spectrum. Another benefit of this system is that it allows for the characterization of resist underlayers. Underlayers are EUV-absorptive layers deposited underneath the resist layer for the purpose of generating additional electrons that feed back into the resist, a process that can be directly measured by the condensed phase electron spectrometer.

Resonant soft X-ray scattering

In addition to EUV light, CXRO is also harnessing the power of synchrotron photons in the soft X-ray energy range to study the relationship between the chemistry and structure of resists after they have been exposed, but before they are developed. This is the latent stage in the EUV lithography process where the critical dimensions in the patterned structure begin to be defined, but they can be particularly difficult to characterize in a non-invasive, non-destructive manner. Resonant soft X-ray scattering can image these latent structures by leveraging the differences in resist chemistry induced by the exposure step in order to enhance scattering contrast between the exposed and unexposed regions. The resulting scattering data can then be used to extract the average latent image 3D profile of the exposed pattern with sub-nm precision. This capability can help uncover the relationships between the chemical profiles within the resist and critical parameters in the final developed structure, such as line edge roughness. Moreover, recent work has shown that this approach can be applied in a reflection geometry, enabling the probing of patterned resist structures directly on standard silicon substrates using a variety of soft X-ray energies [9]. This latest development opens up many possibilities for probing chemical contrast using relevant elemental edges across a broad range of novel resist materials.

SHARP: An actinic mask review microscope

Actinic mask review continues to be a key component of the EUV mask manufacturing process. Mask review tools are designed to emulate the optical geometry of a production EUV scanner so that the recorded aerial image exactly represents, up to a scale factor, the light intensity distribution at the wafer. Not only do these aerial images provide key insights into how defects at the mask transfer to the wafer, they also enable the study of 3D mask effects, pattern architectures, optical proximity

correction, phase-shifting patterns, and more.

The SHARP High-NA Actinic Reticle review Project (SHARP) microscope is a full-field actinic mask review microscope that uses a synchrotron bend magnet source at Beamline 11.3.2 of the Advanced Light Source. The microscope was commissioned in 2013, but due to its flexible zone plate-based optical imaging, is designed to extend to next-generation lithography, supporting resolutions that can image feature sizes at the mask of 32 nm half pitch and beyond.

SHARP, like the MET5, features a lossless Fourier-synthesis illuminator capable of generating arbitrary pupil fills. These pupil fills define the illumination coherence of the imaging system, which affects the appearance of defect repairs and printability, multilayer and line-edge roughness, optical proximity corrections, and the basic properties of contrast and image slope for patterns, especially at small sizes. Data from SHARP are used to calibrate modeling and to provide aerial image information for comparison with wafer printing.

The SHARP objective lenses are diffractive zone plate optics, which are fabricated onto a single chip with electron-beam lithography in a freestanding nickel absorber membrane, shown in Figure 2. A typical SHARP zone plate chip has between 60 and 70 zone plate lenses on it with varying optical properties. Like an optical microscope with an objective turret, the zone plate lenses are designed to be easily interchanged in-situ to support a variety of imaging schemes.

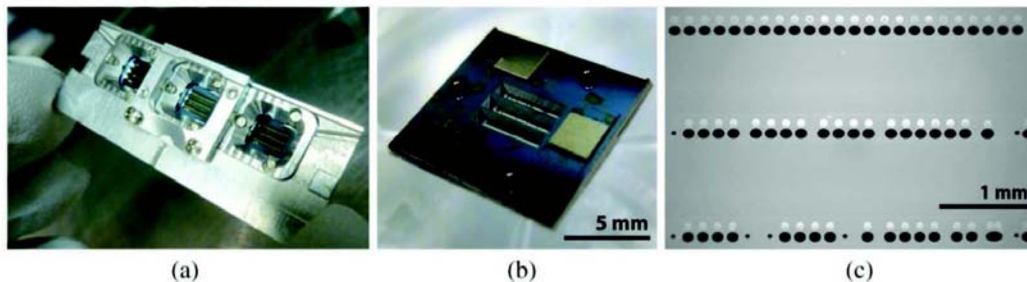

Figure 2: (a) The SHARP zone plate chip holder showing three chips; (b) a close-up of a single zone plate chip with ruby balls as a kinematic coupling mechanism; (c) an SEM image of the zone plate chip showing the zone plates (lighter color) and windows (darker color).

Examples include 4×NA values ranging from 0.25 to 0.625 and five separate azimuthal angles between –25° and +25° to reproduce a rotating plane of incidence across the aperture of a ring-field system characteristic of production EUV scanners. In addition, the chip includes Zernike phase contrast zone plates for phase imaging, as well as zone plates with programmed aberrations for testing image-based wavefront retrieval techniques.

The principal change to the EUV scanner optical geometry to support the next generation of EUV lithography will be the move from the current 0.33 NA isomorphic imaging to 0.55 NA anamorphic imaging. Likewise, the demagnification will move from 4X isomorphic to 4X by 8X anamorphic. As a result, the mask-side NA will be different for the shadowed (0.55/8) and non-shadowed (0.55/4) directions. To accommodate this anisotropic NA, SHARP has been upgraded to include elliptical pupil zone plates [10]. Since SHARP is a single-lens optical system, it is not possible to create true anamorphic magnification; however, the elliptical pupils properly capture the asymmetric numerical apertures and resolution, and the magnification can be emulated in software.

Figure 3 shows an SEM image of an elliptical zone plate lens with asymmetric numerical apertures along its short and long axes, as well

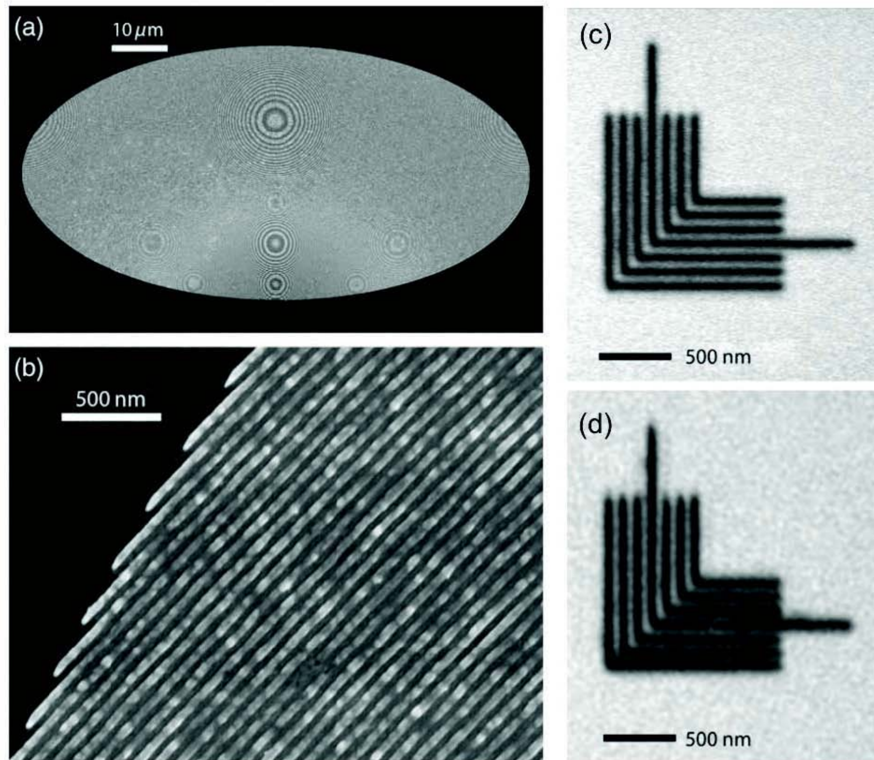

Figure 3: SEM images of (a) a zone plate lens with an anamorphic aperture; (b) a detail image showing the outer zones; (c) a SHARP image of a 50 nm elbow test pattern with an isomorphic zone plate; (d) the same image taken with an anamorphic zone plate showing asymmetric resolution in the horizontal and vertical directions.

as a SHARP image of an elbow pattern demonstrating the asymmetric resolution along the horizontal and vertical axes, characteristic of next-generation anamorphic EUV systems.

The Reflectometer: EUV mask metrology through scatterometry

The CXRO Reflectometer is well-known throughout the EUV and X-ray communities as the standard for material reflectivity characterization. Commissioned in 1995 on the bend magnet Beamline 6.3.2 of the ALS, the Reflectometer was built with a monochromator to achieve bandwidths down to 1/7000 and a sample holder and calibrated photo-diode on a rotation stage to measure reflectivity as a function of angle. Originally conceived as a tool to measure early EUV projection lithography coatings, the Reflectometer has become an indispensable tool for multilayer characterization in the EUV and soft X-ray regimes. Today, the Reflectometer features a 2D rotation stage so that a full 2π-steradian scatter spectrum can be obtained from a sample in reflection or transmission. This capability has opened the door to a wealth of new experiments in EUV mask scatterometry.

As next-generation EUV lithography and inspection systems feature higher numerical apertures, it becomes increasingly important to consider EUV mask 3D effects. These effects include the phase imparted by multilayer reflection, mask shadowing, and the impact of phase absorbers and multilayer etching in phase shift masks. Creating accurate lithographic models for use in source-mask optimization or process window analysis requires an accurate description of the effective complex mask amplitude function.

EUV scatterometry has emerged as a promising candidate for performing actinic mask metrology. An analysis of scatter spectra from targets on an EUV mask while scanning through incident angle and wavelength can reveal information about the mask complex amplitude function. CXRO has developed parametric and nonparametric methods for characterizing the multilayer stack itself, as well as the duty cycle and absorber height of grating-based targets [11]. In the parametric-based methods, the dimensionality of the problem is fixed by a finite set of parameters; in the case of the multilayer stack, these could represent the thicknesses of the individual layers, and in the case of the grating targets, these might be properties like the absorber height and duty cycle. These parameters are then fit onto the measured data until an acceptable fit has been found.

Nonparametric techniques have also been effective on the scatterometry data. For characterizing the multilayer stack, a machine learning algorithm aims to solve for the complex amplitude and phase of the reflectance function as a function of angle, sidestepping the problem of solving for the individual layer thicknesses. For solving for the complex amplitude of masks, a mathematical model is developed that reduces the interaction of the incident wave onto a grating pattern target as a combination of diffraction, reflection, and diffraction, where the effective reflection plane is located below the mirror surface. By matching this model to rigorous RCWA simulations, the location of the reflection plane can be determined, and the complex mask amplitude function can be solved.

High-NA wavefront sensing

Characterizing and removing optical aberrations remain key parts of achieving ultimate resolution in EUV exposure and inspection tools. The primary means for measuring wavefronts in current-generation EUV tools is Lateral Shearing Interferometry (LSI), a common-path interferometric technique that is relatively simple to integrate into most optical geometries. In LSI, a diffraction grating is placed in the beam near the optical system focus. This grating splits the beam into multiple orders, which mutually interfere at the detector. The resulting interferograms contain information about the derivatives of the wavefront in the x-and y-directions, which are used to reconstruct the wavefront using a least squares approach.

As EUV progresses toward higher numerical apertures, the conventional LSI approach breaks down due to nonlinear effects associated with the high incident angles on the grating. At CXRO, the High-NA Wavefront Sensing program was launched to address the challenge of measuring aberrations in high-NA tools. The two main thrusts of this

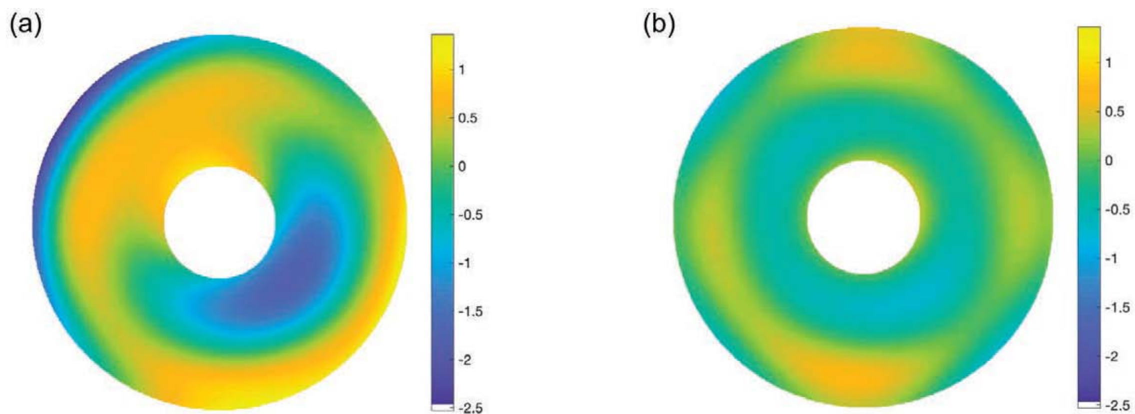

Figure 4: Wavefront of MET5 optic showing aberrations pre-alignment (a) of 0.87 nm rms; and post-alignment (b) of 0.31 nm rms.

program are a version of LSI that is adapted to work at high NA and a new aerial image contrast-based wavefront sensor called the Laplacian Wavefront Sensor (LWS).

High-NA lateral shearing interferometer

When LSI is performed at low to medium NA (<0.3), the interference between adjacent diffraction orders takes the form of a difference function: $\boldsymbol{W(x + s) - W(x)}$, where the shear $\boldsymbol{s}$ is set by the grating pitch and determines the sensitivity of the measurement. $\boldsymbol{s}$ is approximately constant for low incident angles, so this difference approximates the derivative of the wavefront in the direction of the shear, and measuring it in both the x-and y-directions gives sufficient information to reconstruct the wavefront. At high NA (>0.3), the variation of $\boldsymbol{s}$ across the pupil becomes non-negligible due to the large range of incident angles at the grating, and the measured interferogram no longer approximates the wavefront derivative with the same level of accuracy [12].

This problem can be overcome by building a numerical model that captures the nonlinearities of the grating diffraction spectrum. In this model, wavefronts containing various aberration signatures are propagated through the system numerically,

forming a basis of interferograms that represent the system response to each aberration. This basis is built to accommodate a subset of reconstructable aberrations, typically Zernike polynomials through order 37. Measured interferograms are then fit to these basis vectors to reconstruct the wavefront. While this method requires that the numerical model accurately represent the optical geometry of the tool to prevent systematic errors, it is applicable in a wider range of geometries than its conventional counterpart, such as non-telecentric optical systems like the MET5 where the image plane is not normal to the optical axis.

High-NA LSI was implemented as part of the commissioning and optical alignment of MET5, and at 0.5 NA represents the highest numerical aperture EUV optic that has ever been actinically measured. The initial characterization of the wavefront was recorded at 0.87 nm rms ($Z_4 - Z_{37}$) of wavefront error at the center of the field. The aberration profile was analyzed and translated into alignment directives for the optic. After alignment, the aberrations were measured again and were found to have been reduced to 0.31 nm rms, which was below the acceptance specification of 0.5 nm rms.

Lapacian Wavefront Sensor

The Laplacian Wavefront Sensor (LWS) is an image-based method that relies on measuring the contrast of line-space patterns through focus. The working principle is based on the idea that aberrated wave-fronts have localized curvature variations that produce well-defined focus shifts of mask targets as a function of illumination. These targets are typically equal line/space grating patterns, and monopole illumination is used to ensure that exactly three diffracted orders are accepted by the pupil so that the functional form of the resulting contrast curves is parabolic, allowing best-focus to be determined with high accuracy. Each combination of grating (pitch and orientation) and illumination constitutes a wavefront curvature "probe," and library of focus shifts

Table 1: LWS-reconstructed aberrations.

Aberration	**RMS reconstruction error**
Astigmatism XY (Z_5)	2.14 mλ (28.9 pm)
Coma X (Z_7)	4.89 mλ (66.0 pm)
Spherical (Z_9)	4.66 mλ (62.9 pm)
Linear combination ($Z_5 - Z_9$)	4.16 mλ (56.2 pm)

as a function of probe is precomputed for each Zernike polynomial. An operator is constructed by inverting this library that reconstructs the wavefront from focus shifts measured experimentally.

In order for the reconstruction to be well-posed, the number of probes should be larger than the number of Zernikes in the reconstruction. Also, the diversity of probes must be large enough so that the signatures of the Zernike polynomials in the reconstruction are sufficiently distinct. Mathematically, this condition can be expressed as the requirement that the condition number of the reconstruction operator be sufficiently low. In practice, LWS works best when reconstructing on a small number of Zernike polynomials, such as the primary aberrations: primary astigmatism, primary coma, and primary spherical aberration. Such a situation arises frequently in EUV optical systems where the optics of a multi-optic system are individually high-quality, but the system as a whole has aberrations due to alignment error. This constraint notwithstanding, LWS often requires little to no system integration, since it works based on existing imaging, is independent of numerical aperture, and is extremely accurate, since best-focus is largely insensitive to noise.

LWS was tested on the SHARP microscope using zone plates with known, programmed aberrations. Each zone plate is designed to contain 50 or 100 mλ (0.675 or 1.35 nm) of astigmatism (*xy* and 45°), *x*-and *y*-coma, spherical aberration, or a linear combination of these in known proportions. Aerial images were collected on the SHARP CCD in normal imaging mode, using an NA of 0.33/4, and 12 probes. For each probe, 16 images were taken through focus with focus steps of 100 nm. Aberrations were reconstructed in all cases to better than 5 milliwaves (λ/200), as shown in the Table 1.

Both high-NA LSI and LWS represent viable wavefront sensing techniques for next-generation EUV tools with high numerical aperture optical systems. The choice of using one technique over the other depends on the needs of the system as well as the ease of integration. High-NA LSI is better at reconstructing a larger number of Zernike polynomials with far less data acquisition; however, it requires the integration of a grating and CCD. LWS is robust against noise and can measure low-order Zernike polynomials with extremely high accuracy and precision, but requires more data collection due to the multiple through-focus series and precise illumination control, and therefore may not be optimal for systems requiring high-order Zernike reconstruction.

Summary

The next generation of EUV lithography will require a concerted effort by the EUV scientific community in order to overcome the many challenges on the horizon. EUV activities at CXRO play an important role in this effort. The 0.5 NA MET5 has already shown print resolution of 8-nm half pitch, allowing resist chemists to test properties of new EUV resists at next-generation resolution. Radiation chemistry studies are underway to shed light on the mechanisms of primary and secondary electrons in EUV resists. Anamorphic-emulated zone plates in SHARP provide full-field aerial images at the numerical aperture of next-generation scanners. The Berkeley Reflectometer is being used to characterize EUV mask 3D properties using novel machine-learning algorithms. And two viable high-NA wavefront sensing techniques have been developed—high-NA LSI and LWS—for measuring next-generation imaging and exposure tools. High-NA LSI has already been used to characterize the 0.5 NA Schwarzschild optic in the MET5, the highest numerical aperture actinic measurement of an EUV optic. As the semiconductor industry transitions to the next generation of EUV, CXRO is committed to deploying its resources to advance EUV science and push the technology forward toward high-volume manufacturing.

References

H. J. Levinson et al., *Proc. SPIE 10809*, International Conference on Extreme Ultraviolet Lithography 2018, October 24, 1080903 (2018).
E. van Setten et al., *Proc. SPIE 10957*, Extreme Ultraviolet (EUV) Lithography X, March 26, 1095709 (2019).
I. Mochi et al., *J. Micro/Nanolith. MEMS MOEMS* **18**(1), 014002 (2019).
D. De Simone et al., *Proc. SPIE 10143*, Extreme Ultraviolet (EUV) Lithography VIII, March 24, 101430R (2017).
C. Anderson et al., *Proc. SPIE 10957*, Extreme Ultraviolet (EUV) Lithogra phy X, March 26, 1095708 (2019).
J. van Schoot et al., *J. Micro/Nanolith. MEMS MOEMS* **16**(4), 041010 (2017).
O. Kostko et al., *Proc. SPIE 10450*, International Conference on Extreme
Ultraviolet Lithography 2017, October 16, 104500J (2017).
J Ma et al., *Proc. SPIE 10957*, Extreme Ultraviolet (EUV) Lithography X, May 30, 109571Y (2019).
G. Freychet et al., *J. Micro/Nanolith. MEMS MOEMS* **18**(2), 024003 (2019).
M. Benk et al., *J. Micro/Nanolith. MEMS MOEMS* **15**(3), 033501 (2016).
S. Sherwin et al., *Proc. SPIE 10809*, International Conference on Extreme Ultraviolet Lithography 2018, October 3, 108090T (2018).
W. Zhu et al., *Proc. SPIE 10809*, International Conference on Extreme Ultraviolet Lithography 2018, October 9, 108091S (2018).